Earthquakes and Structures, *Vol. 17, No. 1 (2019) 39-48*
DOI: https://doi.org/10.12989/eas.2019.17.1.039

Study on seismic performance of steel frame with archaized-style under pseudo-dynamic loading

Zuqiang Liu*, Chaofeng Zhou and Jianyang Xue

School of Civil Engineering, Xi'an University of Architecture and Technology, Xi'an 710055, China

(Received October 15, 2018, Revised April 9, 2019, Accepted April 13, 2019)

Abstract. This paper presents an experimental study on a 1/2 scale steel frame with archaized-style under the pseudo-dynamic loading. Four seismic waves, including El Centro wave, Taft wave, Lanzhou wave and Wenchuan wave, were input during the test. The hysteresis characteristic, energy dissipation acceleration response, displacement response, strength, stiffness and strain were analyzed. Based on the experiment, the elastoplastic dynamic time-history analysis was carried out with the software ABAQUS. The stress distribution and failure mode were obtained. The results indicate that the steel frame with archaized-style was in elastic stage when the peak acceleration of input wave was no more than 400 gal. Under Wenchuan wave with peak acceleration of 620 gal, the steel frame enters into the elastoplastic stage, the maximum inter-story drift was 1/203 and the bearing capacity still tended to increase. During the loading process, Dou-Gong yielded first and played the role of the first seismic fortification line, and then beam ends and column bottom ends yielded in turn. The steel frame with archaized-style has good seismic performance and meets the seismic design requirement of Chinese code.

Keywords: archaized building; steel frame; pseudo-dynamic test; seismic performance; elastoplastic time-history analysis; dynamic response

1. Introduction

Chinese ancient architectures, with high historical value and scientific value, are the crystallization of the long historical culture of Chinese nation. It has an important influence on architecture of many countries, especially in Japan and South Korea. Most of Chinese ancient architectures are made of wood and have a special connection method "mortise-tenon". Researches indicate that the Chinese ancient wooden structure can show perfect seismic performance through the energy dissipation of column base and mortise-tenon (Jiang *et al*. 2016, Zhang *et al*. 2011). However, as time goes on, due to the various influencial factors (such as natural disasters, human activities), most of the ancient buildings have disappeared. Only a few ancient wooden structures are well preserved in China, such as Yingxian Wooden Pagoda, as shown in Fig. 1.

In order to inherit the precious cultural heritage, the archaized building was put forward, which combines modern materials and construction techniques with ancient architecture culture connotation (Wang 2012). It not only carries forward the traditional Chinese culture, but also has excellent seismic performance and meets the modern functional requirements. Therefore, a large number of archaized buildings have been built in recent years, such as Chang'an Tower (Fig. 2), which is the landmark building of Xi'an International Horticultural Exhibitions.

Fig. 1 Yingxian Wooden Pagoda

Fig. 2 Chang'an Tower

At present, the research on archaized buildings mainly focuses on the wood structure (Gattesco and Boem 2015, Parisi and Piazza 2015). However, due to the material defects of the wood, the wood structure cannot be applied in many places. Steel structure has light weight, high bearing capacity and good ductility (Cheng and Wen 2017, Ghasem 2018, Li *et al*. 2018, Lian *et al*. 2017, Wang *et al*. 2014,

*Corresponding author, Associate Professor
E-mail: liuzuqiang@xauat.edu.cn

ISSN: 2092-7614 (Print), 2092-7622 (Online)

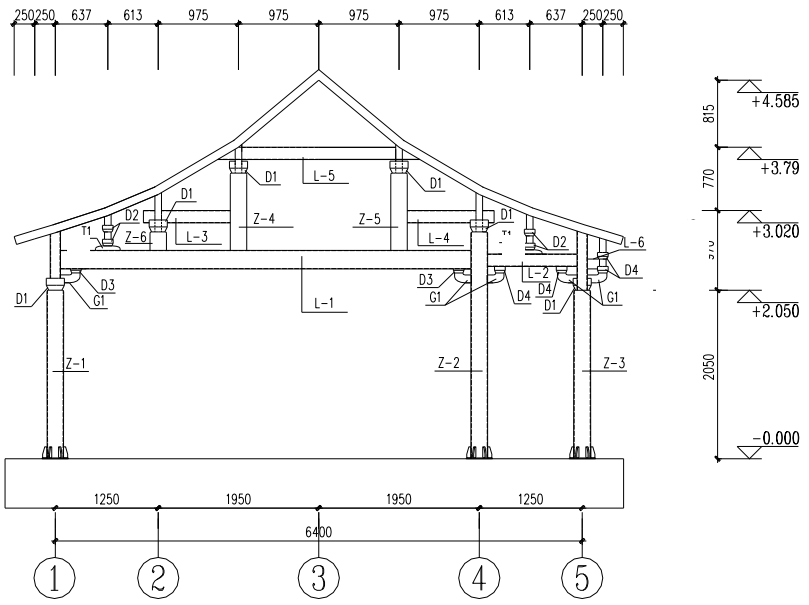

Fig. 3 Dimensions of the specimen

Negin *et al*. 2017, Dan 2008, Blum *et al.* 2019, Sakr *et al*. 2019), and it is easy to construct. Therefore, the steel structure with archaized-style becomes popular all over the world, especially in China. At present, lots of researches on steel structure with archaized style are conducted in China. Wu (2010) introduced the concept of architecture and the design of structure about Dingding Luoyang gate, and analyzed the static elastoplastic characteristic. The results showed that the gate tower had good seismic performance under the earthquake with magnitude of 7-degree, but the performance could be affected by the construction sequence. Qi *et al*. (2017) examined experimentally the behavior of transition steel connections between smaller rectangular and larger circular tubes in traditional-style Chinese buildings under different axial compression ratios and slenderness ratios. The results indicated that the steel connections had good seismic performance, and the primary failure modes included cracking of welds or base metal around the welds and local buckling of the flange at the base of the rectangular steel tube column. Xue *et al*. (2018) performed influence analysis of bracket set on seismic performance of steel eave columns in Chinese traditional style buildings. The results showed that the seismic performance of specimens with bracket set was better than that of the specimens without bracket set. Xue *et al.* (2015) carried out an experimental research on the double beam-column joints in traditional steel structures under the cyclic reversed loading. The test results indicated that three core zones, including upper, middle and lower core zone, were formed in the traditional inner joints during the loading process, and the plastic deformation mainly occurred in the lower core zone.

It can be seen that the researches mentioned above can only reveal the performance of local steel structure with archaized-style. There are few researches on integral steel structure with archaized-style, which results in that the steel structures with archaized-style can only be designed based on experience and related immature regulations. Therefore, it is difficult to ensure the safety of the structure. This paper presented an experimental research on a planar steel frame with archaized-style under the pseudo dynamic loading. The seismic performances, including hysteretic behaviors, energy dissipation, strength, stiffness and dynamic responses, were analyzed. Based on the experiment, a finite element analysis was carried out, and the failure mode and stress distribution were investigated.

Table 1 Dimensions of main components

Components	Specimen ID	Section
Column	Z-1, Z-3	Lϕ203×6 U□125×5
	Z-2	ϕ203×6
	Z-4, Z-5, Z-6	□125×3
Beam	L-1	□225×125×3
	L-2, L-3, L-4, L-5	□150×100×3
	L-6	□120×100×3

2. Experimental program

2.1 Specimen design

The prototype structure, a two-span and single-story steel frame with archaized-style, is located in the seismic fortification zone of intensity 8. Considering the test conditions, the structural scale was chosen as 1/2, and the dimension of model is shown in Fig. 3, in which *Z*, *L*, *D* and *G* represent column, beam, Dou and Gong, respectively.

The components of steel frame were manufactured in the factory and assembled in the laboratory. The cross-section dimensions of beams and columns are shown in Table 1, in which the letter "*L*" and "*U*" represents the lower column and upper column. As shown in Fig. 4, the upper column was inserted into the lower column and both of them were connected by four vertical stiffeners, which were rectangular plates and welded on the outside of upper

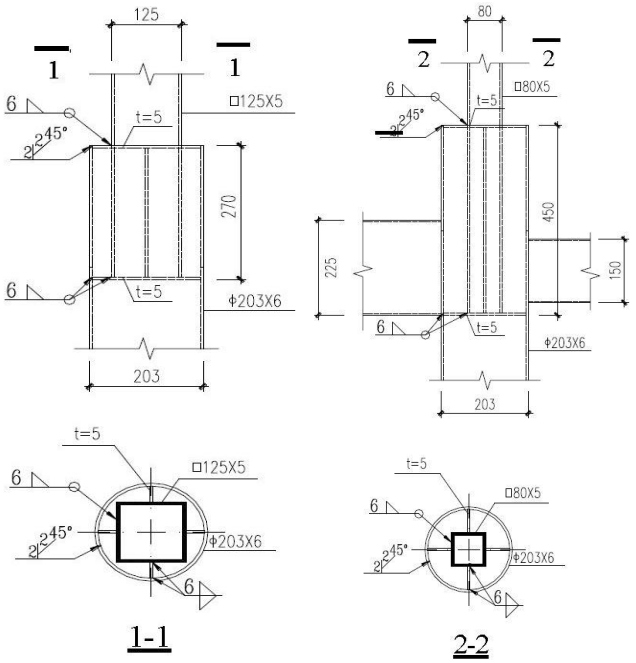

(a) Columns Z-1 and Z-3 (b) Column Z-2

Fig. 4 Connection of the lower column and the upper column

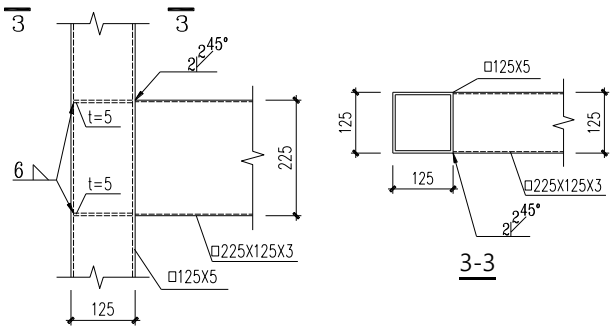

Fig. 5 Connection of column Z-1 and beam L-1

column and the inside of inside column. There were two circular ring plates welded on the inside of lower column, one was at the bottom of upper column and another with a rectangular hole was at the top of lower column. The beam and column were connected by the full penetration weld, and two horizontal stiffeners were welded on the inside of column corresponding to the top and bottom flanges of beam, as shown in Fig. 5. The open column foot with fixed constraint was adopted, as shown in Fig. 6. Six stiffened plates and one bottom plate were welded on the outside of column, and the bottom plate was fixed on the foundation by the high-strength bolts. Dou and Gong were welded by using plates of 3mm, of which the dimensions are shown in Fig. 7. The grade of steel was Q235B, and the result of the material test is shown in Table 2.

According to the capacity of test device and material properties, the similarity coefficient of length, elastic modulus and acceleration for the model was chosen as 1/2, 1 and 1, respectively. And then the other coefficients can be derived by the dimension analysis method. The major similarity relationship is shown in Table 3.

Table 2 Mechanical indexes of steel

Materials	Thickness t/mm	Yield strength f_y/MPa	Ultimate strength f_u/MPa	Elastic modulus E_s/MPa
Plates	3	327.3	476.8	2.12×10^5
	5	317.6	390.7	2.04×10^5
	10	289.2	407.1	1.89×10^5
Tubes	3	335.9	502.4	2.11×10^5
	6	306.3	362.6	1.90×10^5

Table 3 Similarity coefficients

Parameter	Symbol	Equation	Value
Length	L	$S_L = L_m / L_p$	1/2
Area	A	$S_A = S_L^2$	1/4
Displacement	x	$S_x = S_L$	1/2
Stress	σ	S_σ	1
Strain	ε	$S_\varepsilon = S_\sigma / S_E$	1
Young's modulus	E	S_E	1
Force	F	$S_F = S_L^2 S_E$	1/4
Mass	m	$S_m = S_L^2 S_\sigma$	1/4
Time	t	$S_t = (S_\sigma S_L / S_E)^{1/2}$	$\sqrt{1/2}$
Frequency	f	$S_f = [S_E / (S_L S_\sigma)]^{1/2}$	$\sqrt{2}$
Acceleration	a	$S_a = S_E / S_\sigma$	1

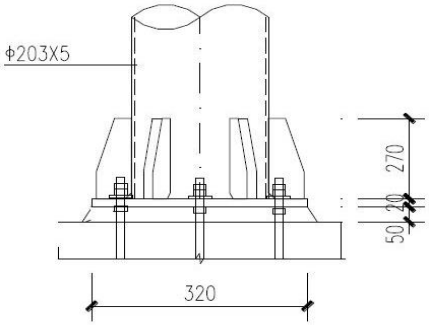

Fig. 6 Open column foot

2.2 Loading scheme

The single-degree-of-freedom pseudo-dynamic test method was adopted for the test. The fixed foundation of the specimen was a rigid base of the reinforced concrete beam with 7500 mm×500 mm×600 mm (length×width× height), which was fixed to the geosyncline through the anchor bolt slot. Two lateral supports were used to limit the out-plane deformation of the specimen. A 500 kN electro-hydraulic servo actuator was placed at the elevation of 2422 mm. The loading layout of the test is shown in Fig. 8.

The vertical load was carried out by using the concrete counterweight on both sides of the steel frame with the cable suspension, as shown in Fig. 8. The concrete counter weight was lifted first to apply the vertical load. Then, the horizontal load was applied to obtain the initial stiffness matrix. Finally, the pseudo-dynamic loading test was carried out by stepwise loading method.

Considering the characteristic of the site at which the prototype locates, El Centro wave (1940), Taft wave (1952), Wenchuan wave (2008) and Lanzhou wave were chosen. The time interval Δt of El Centro wave, Taft wave and

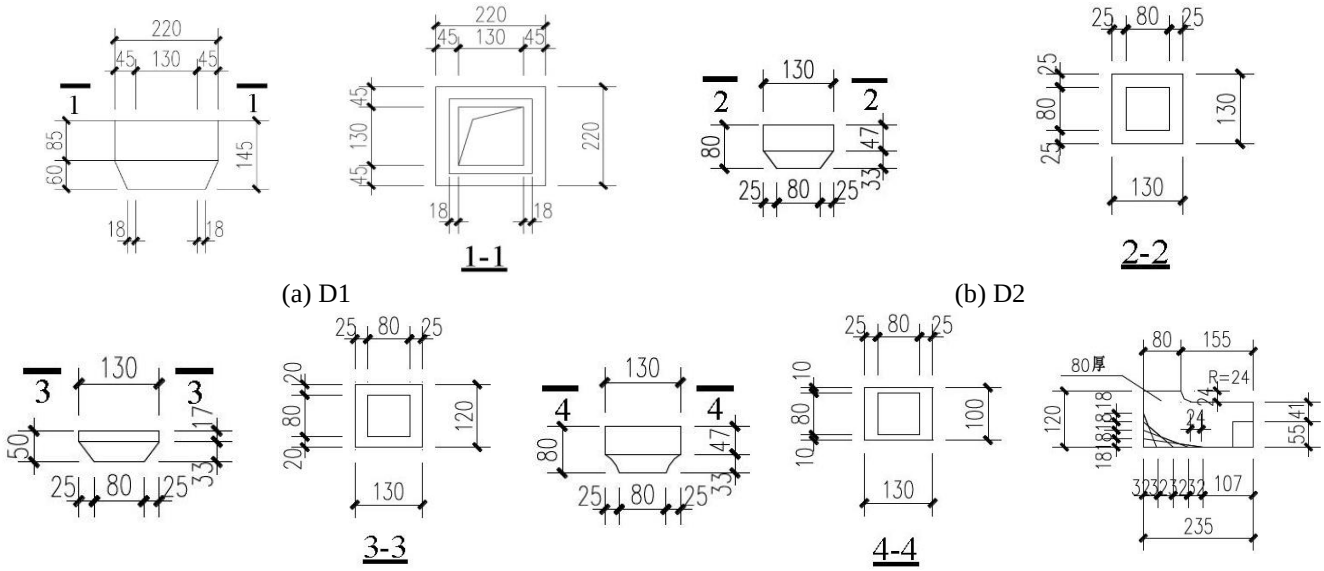

(a) D1 (b) D2

(c) D3 (d) D4 (e) G1

Fig. 7 Dimensions of Dou and Gong

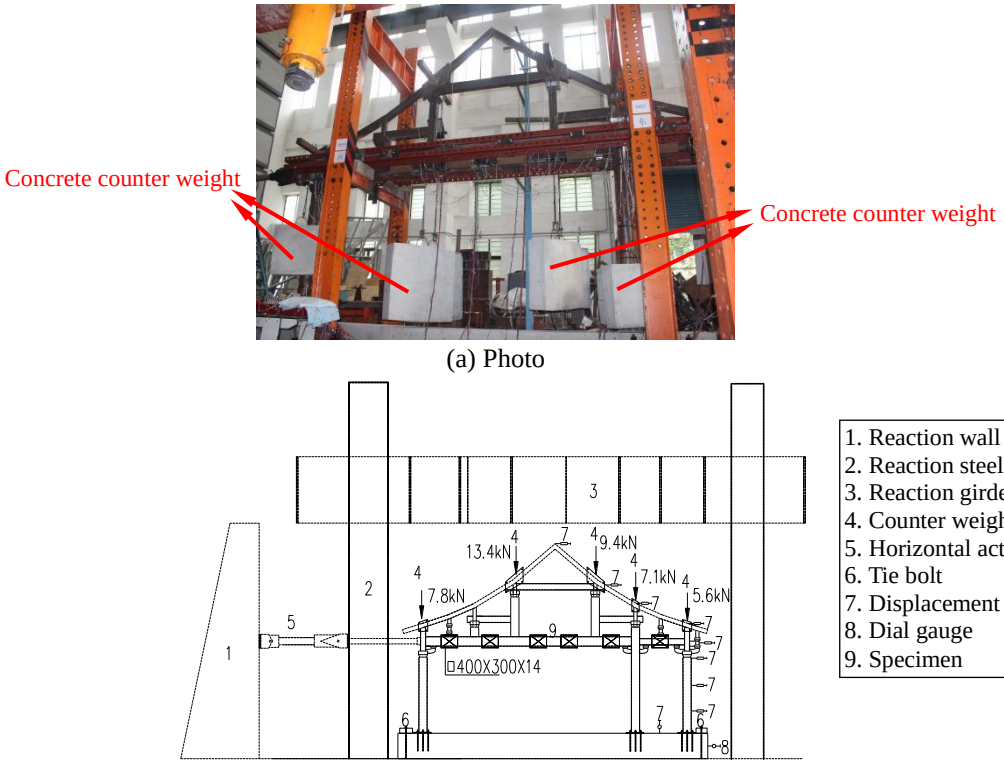

(a) Photo

(b) Setup

Fig. 8 Test devices

Lanzhou wave was reduced to 0.014s according to the similarity ratio, and 1000 points from the original seismic waves were taken as the input wave, so the duration of input waves was 14s after reducing. The time interval Δt of Wenchuan wave was reduced to 0.0035s according to the similarity ratio, and 4000 points from the original seismic wave were taken as the input wave, so the duration of input waves was 14s after reducing. The loading conditions are listed in Table 4.

2.3 Measuring points

78 strain gauges and 4 strain rosettes were used to measure measure the strain changes of components. Strain gauges were mainly arranged on the column ends, beam ends and Dou-Gong. Strain gages of beam ends were on the center line of the top and bottom surfaces. Strain gauges of column ends were on the center line of surfaces perpendicular to the loading direction. Strain rosettes

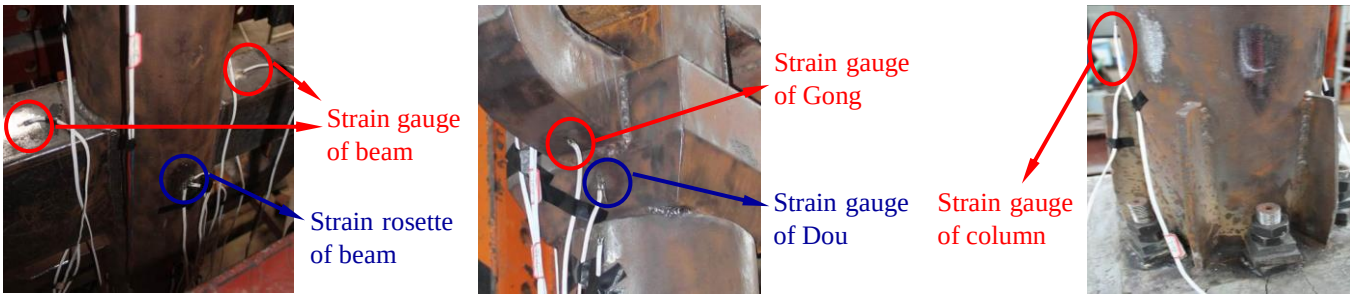

(a) Connection of column Z-2 and beams (b) Dou-Gong of column Z-3 (c) Bottom end of column Z-3

Fig. 9 Arrangement of strain gauges and rosettes

Table 4 Loading conditions

Condition	Seismic wave	Peak acceleration(gal)
1	El Centro wave	70
2	Taft wave	70
3	Lanzhou wave	70
4	Wenchuan wave	70
5	El Centro wave	200
6	Taft wave	200
7	Lanzhou wave	200
8	Wenchuan wave	200
9	El Centro wave	400
10	Wenchuan wave	400
11	Wenchuan wave	620

were pasted on the core joints. Fig. 9 shows the arrangement of the strain gauges and rosettes.

3. Test results and analysis

3.1 Test phenomenon

Fig. 10 Deformation of Dou-Gong of column Z-3 after test

Under four seismic waves, including El Centro wave, Taft wave, Lanzhou wave and Wenchuan wave, with peak accelerations of 70 gal and 200 gal, all components of the frame did not yield, and the welds did not crack. Every component was still in good condition. Under El Centro wave and Wenchuan wave with the peak acceleration of 400 gal, the steel frame was basically in the elastic stage and no plastic deformation was found.

Under Wenchuan wave with the peak acceleration of 620 gal, there were no obvious buckling instability and out-of-plane deformation for the frame. The strain data showed that the Dou of Column Z-1 and the Gong of Column Z-2 yielded successively, but the deformation of Dou-Gong was

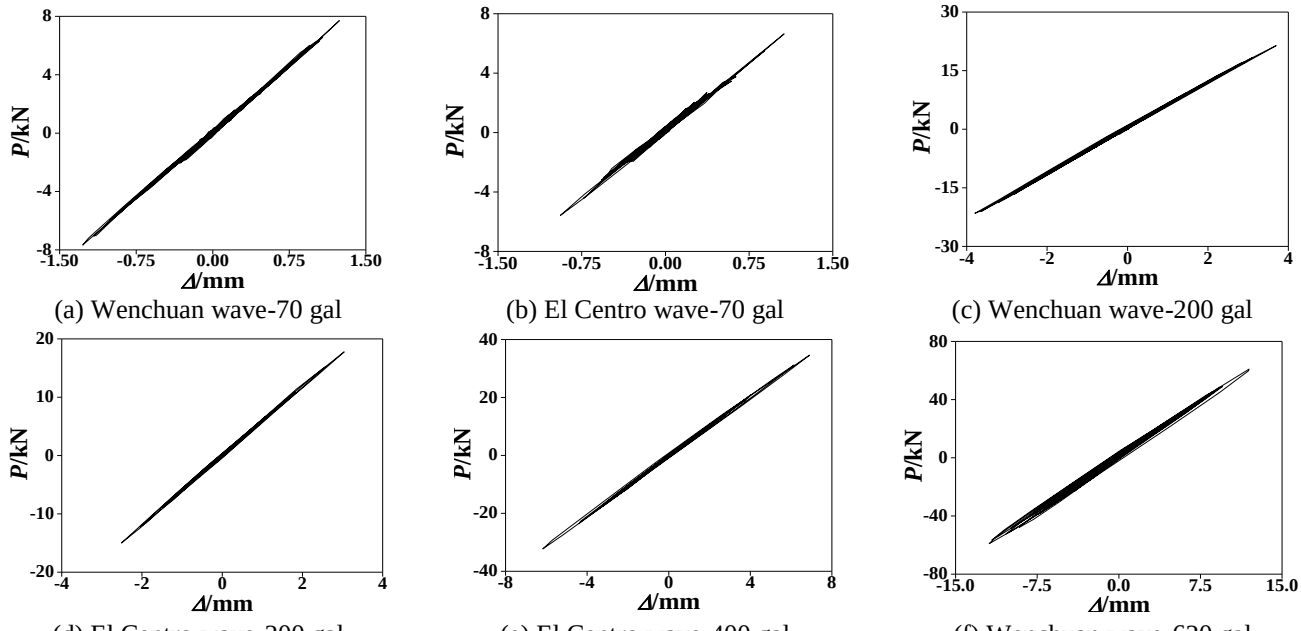

(a) Wenchuan wave-70 gal (b) El Centro wave-70 gal (c) Wenchuan wave-200 gal

(d) El Centro wave-200 gal (e) El Centro wave-400 gal (f) Wenchuan wave-620 gal

Fig. 11 Hysteretic loops of base shear and top displacement

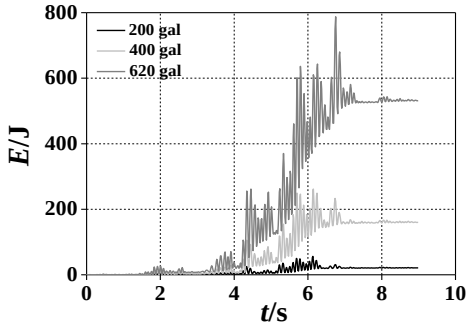

Fig. 12 Hysteretic energy dissipation capacity curves

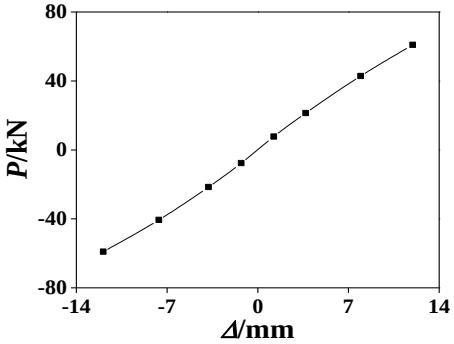

Fig. 13 *P*-Δ skeleton curve

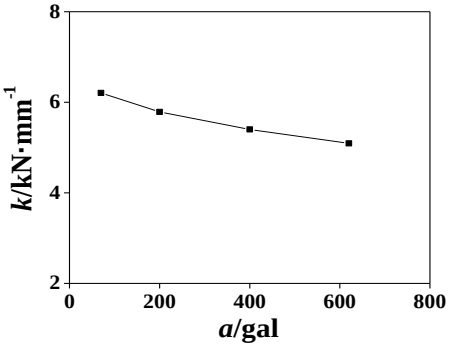

Fig. 14 Stiffness degradation

not obvious, as shown in Fig. 10. There was no significant damage on the whole, indicating that the steel frame with archaized-style has good seismic performance and meets the requirements of seismic fortification.

3.2 Hysteresis characteristics and energy dissipation

Fig. 12 shows the hysteresis curves between the base shear and top displacement under some loading conditions. It can be seen that the steel frame had no obvious decline on the bearing capacity. The area encircled by the hysteresis curves increased with the increase of peak acceleration. When inputting Wenchuan wave with the peak acceleration of 620 gal, the hysteresis curve could not return to the origin in the negative loading, indicating that the steel frame had some residual deformation and entered into the elastic-plastic stage.

In the pseudo-dynamic test, due to the little influence of velocity on the structure, the damping energy can be neglected, and the hysteretic energy dissipation accounts for the majority of input earthquake energy. Fig. 11 shows the time-history curve of energy dissipation under Wenchuan wave with different peak accelerations. The energy dissipation can be calculated according to the Eq. (1), where E represents the accumulated hysteretic energy dissipation, V represents the base shear, x represents the top displacement and t represents the time. As shown in the figure, the energy dissipation increased with the increase of peak acceleration. Under the rare earthquake of intensity 9, corresponding to the peak acceleration of 620 gal, the hysteresis energy increased rapidly because some components of the frame yielded, and it was about 3.3 times than that of rare earthquake of intensity 8, corresponding to the peak acceleration of 400 gal.

$$E(t_i)=\sum_{i=1}^{m}\frac{1}{2}[V(t_i)+V(t_{i-1})][x(t_i)-x(t_{i-1})] \quad (1)$$

3.3 Strength and stiffness

Fig. 13 shows the skeleton curve between base shear and top displacement under Wenchuan wave with different peak accelerations. It can be seen that the base shear increased with the deformation development of the steel frame. When the peak acceleration reached to 620 gal, the maximum inter-story drift was 1/203 and the strength tended to continue growing, which reflects that the steel frame with archaized-style has strong lateral deformation ability and high bearing capacity.

According to the skeleton curve, the stiffness degradation (k) curve is shown in Fig. 14, in which the stiffness is represented by the secant stiffness. It can be seen that with the increase of the peak acceleration, the damage of the steel frame was aggravated and the structural stiffness decreased gradually, which could prolong the fundamental period of the structure.

3.4 Acceleration response

Fig. 15 shows the acceleration response of the loading point under different loading conditions. It can be seen that the shape of acceleration time-history curve was consistent with the corresponding input seismic wave under different seismic waves with the peak acceleration of 200 gal, because the frame was in elastic state. However, the acceleration response and the input seismic wave did not reach to the maximum at the same time. The maximum acceleration of El Centro wave, Lanzhou wave and Wenchuan wave appeared at the time of 1.513s, 3.564s and 8.7646s in the positive direction respectively, while the maximum acceleration response appeared at the time of 1.7779s (in the negative direction), 2.0019s (in the negative direction) and 7.7979 s (in the positive direction) respectively. Under Wenchuan wave, the acceleration response increased with the increase of peak acceleration. When the peak acceleration reached to 600 gal, some components yielded, and the stiffness degradation of the steel frame lead to decrease of vibration frequency, so that the shape of acceleration response curve did not agree with that of input wave.

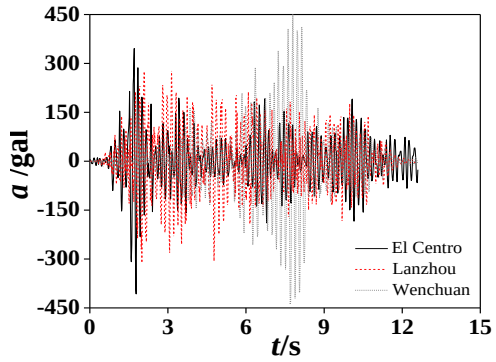

(a) Under the seismic wave with the peak acceleration of 200 gal

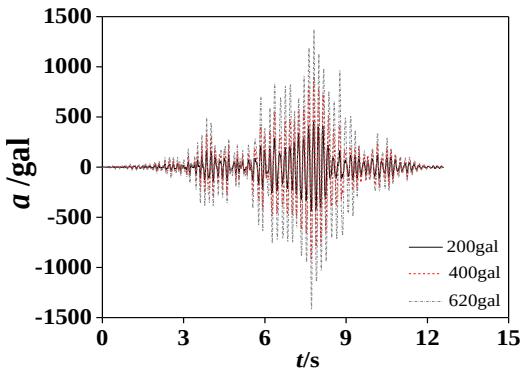

(b) Under the action of Wenchuan wave

Fig. 15 Time history curves of top acceleration

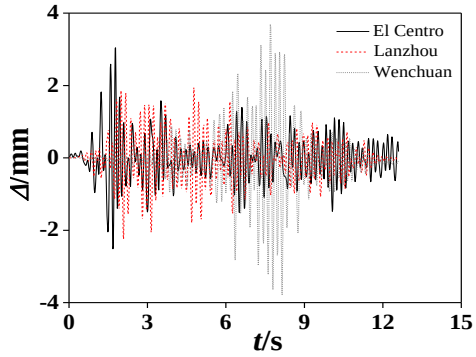

(a) Under the seismic wave with the peak acceleration of 200 gal

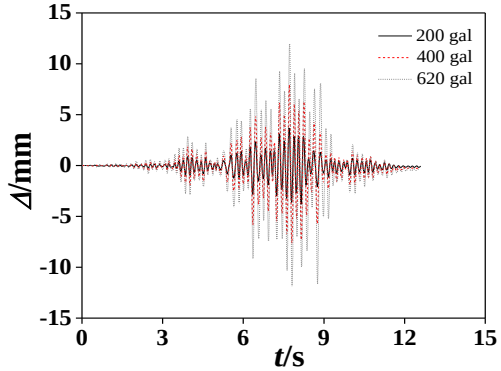

(b) Wenchuan wave with different peak accelerations

Fig. 16 Time history curves of top displacement

3.5 Displacement response

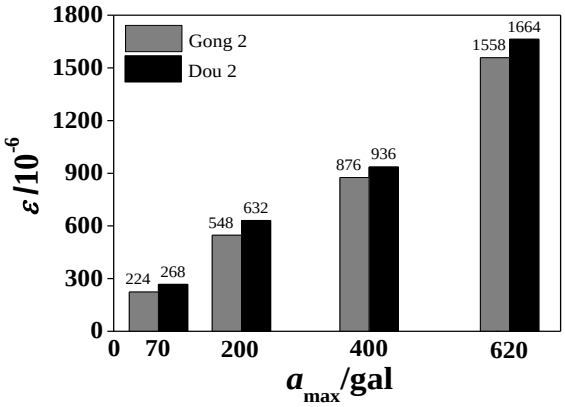

Fig. 17 Strains of D2 and G1

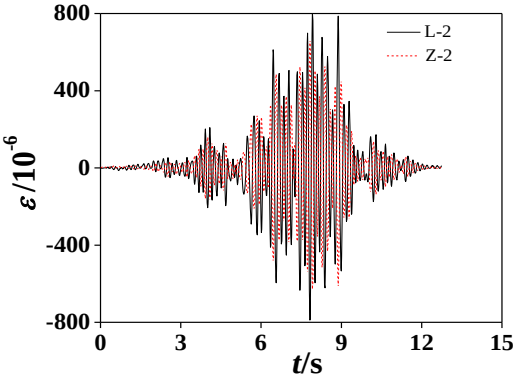

Fig. 18 Strains of beam L-2and column Z-2

The top displacement time-history curves under different loading conditions are shown in Fig. 16. It can be seen that under different seismic waves with the peak acceleration of 200 gal, the time at which the maximum of displacement response appeared was different from that of the peak acceleration of input wave. Wenchuan wave, of which the predominant period is close to the self-vibration period of the steel frame, had the most insignificant influence on the displacement response among the three waves. Under Wenchuan wave, the top displacement response increased with the increase of peak acceleration, but the increasing rate decreased due to the increase of accumulated damage of the structure.

3.6 Strain

Fig. 17 shows the peak strain of D2 and G1 under Wenchuan wave with different acceleration peaks. It can be seen that the strains of D2 and G1 increased continuously with the increase of peak acceleration. When the peak acceleration reached to 620 gal, the strains of D2 and G1 exceeded the yield strain. According to the test data, only D2 and G1 yielded during the loading process, and the other components had not yielded until the test ended.

Fig. 18 shows the strain time-history curve of the L-2 beam end and the Z-2 column end under Wenchuan wave with the acceleration peak of 620gal. As shown in the figure, the strain of beam end is greater than that of column end, but the strains of the both were less than the yield strain, which were $1544\times10^{-6}$and 1612×10^{-6}, respectively.

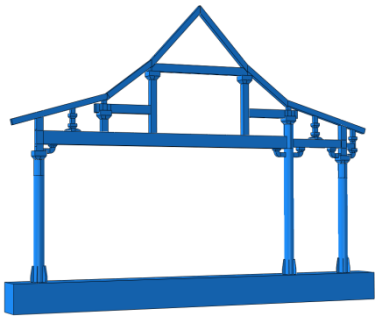

Fig. 19 Finite element model

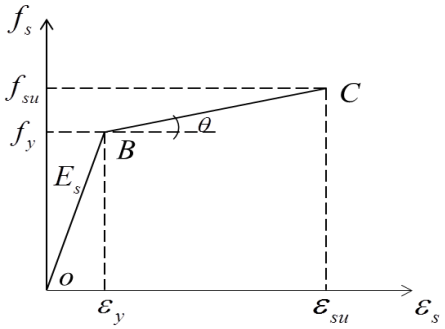

Fig. 20 Bilinear constitutive model

4. Elastoplastic dynamic time-history analysis

4.1 Finite element model

In order to further analyze the stress state and failure mode of the steel frame with archaized-stytle under earthquake, the elastoplastic dynamic time-history analysis was carried out by the software ABAQUS.

The three-dimensional shell element was adopted for the finite element model, as shown in Fig. 19. The Bilinear constitutive model (Fig. 20 and Eqs. (2) and (3)) was used for the strain-stress relationship of steel, and Von-Mises yield criterion was used to judge whether the steel entered into the yield stage. The "Tie" constraint was used to simulate the action of weld, which insured that there was no relative motion between members. It can be seen from the experimental results that the displacement response of Wenchuan wave was the largest. Therefore, Wenchuan waves with different acceleration peaks were selected as the input seismic waves, and the acceleration peaks includes 400 gal, 620 gal, 800 gal and 1000 gal.

$$\sigma_s = E_s \varepsilon_s \quad (\varepsilon_s \le \varepsilon_y) \tag{2}$$

$$\sigma_s = f_y + (\varepsilon_s - \varepsilon_y)\frac{f_{su} - f_y}{\varepsilon_{su} - \varepsilon_y} \quad (\varepsilon_y \le \varepsilon_s \le \varepsilon_{su}) \tag{3}$$

4.2 Comparison of the calculated and experimental results

The displacement responses under Wenchuan waves with the peak acceleration of 400 gal and 620 gal are compared between the calculated results and the experimental results, as shown in Fig. 21, and the comparison of the maximum displacement are shown in Table 5. As shown in Fig. 21 and Table 5, the calculated results basically matched with the experimental results, which indicates that the dynamic time-history analysis of the model is reasonable. The displacement obtained by the experiment was slightly larger than that of the finite element analysis. The reason is that the connection between the specimen and actuator may be loose during the loading process, as well as the actual anchorage of foundation is difficult to achieve the ideal state appearing in finite element analysis.

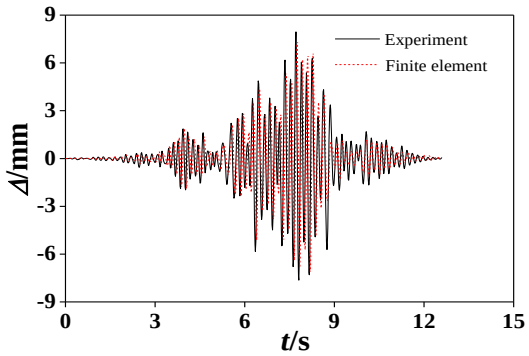

(a) Under Wenchuan wave with the peak acceleration of 400 gal

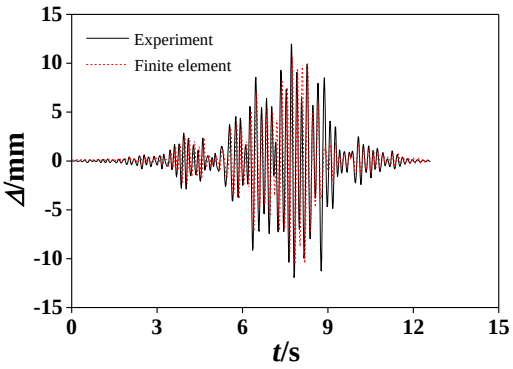

(b) Under Wenchuan wave with the peak acceleration of 620 gal

Fig. 21 Comparison of displacement and time curve

Table 5 Comparison of the maximum displacements

a_{max}/gal	Loading direction	Calculated value Δ_{cal}/mm	Experimental value Δ_{exp}/mm	$\Delta_{cal}/\Delta_{exp}$
400	Positive	7.33	7.94	0.92
400	Negative	-7.13	-7.63	0.93
620	Positive	10.59	11.96	0.88
620	Negative	-10.57	-11.92	0.89

4.3 Weak zones and failure mode

In order to further analyze the weak zones and failure mode of the steel frame, the finite element analysis was carried out under Wenchuan waves with the peak acceleration of 800 gal and 1000 gal.

Under Wenchuan wave with the peak acceleration of 800 gal, the stress distribution of the steel frame at 7.73s is shown in Fig. 22. It can be seen that the stress of Dou-Gong, of which most areas yielded, are larger than that of

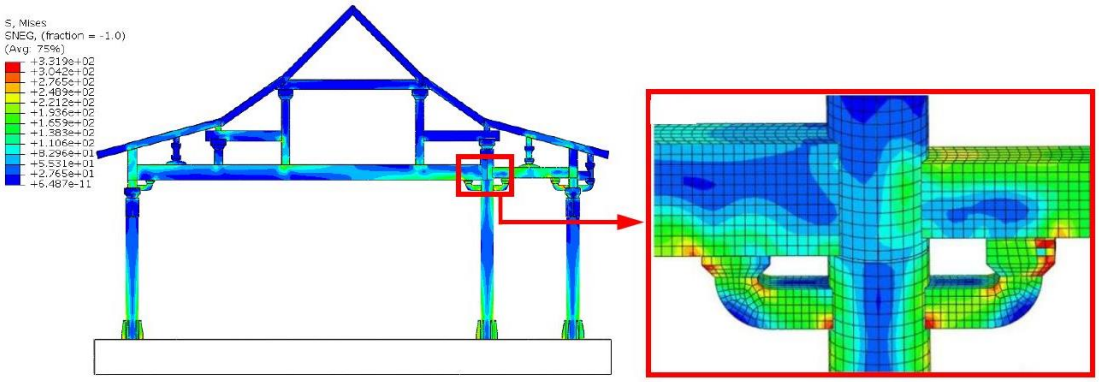

Fig. 22 Stress distribution under Wenchuan wave with the peak acceleration of 800 gal

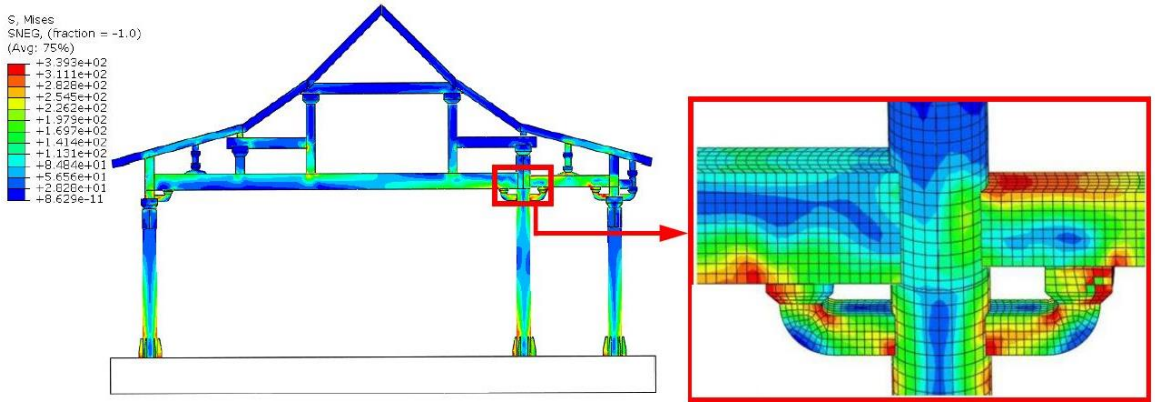

Fig. 23 Stress distribution under Wenchuan wave with the peak acceleration of 1000 gal

the other components.

The bottom flange of beam end near the Dou-Gong of column Z2 yielded partially. However, the stress of column was smaller than the yield stress.

Under Wenchuan wave with the peak acceleration of 1000 gal, the stress distribution at 7.73s is shown in Fig. 23. It can be seen that the plastic deformation of Dou-Gong continued to develop. The beam ends yielded significantly and formed plastic hinges. Some areas of the column bottom end entered into yield stage.

Above analysis demonstrates that Dou-Gong, of which the stress was the largest, yielded first. Following Dou-Gong, the beam ends at both sides of Dou-Gong of column Z-2 yielded and the plastic deformation developed obviously. These zones with large stress are the weak zones of the steel frame. The stress of the column bottom end was smaller than that of beam ends, and the plastic deformation developed slowly. The failure mode meets the seismic requirements of "strong column-weak beam". Dou-Gong plays the role of the first seismic fortification line.

5. Conclusions

This paper presents an experimental research on the steel frame with archaized-style under the pseudo-dynamic loading. Based on the experiment, finite element analysis was conducted. Major conclusions are summarized as follows:

• According to the pseudo-dynamic test, the steel frame was in the elastic stage under El Centro wave, Taft wave, Lanzhou wave and Wenchuan wave with the peak acceleration of less than 400 gal (corresponding to rare earthquake of intensity 8.0). Under Wenchuan wave with the peak acceleration of 620 gal (corresponding to rare earthquake of intensity 9.0), Dou-Gong entered the yield stage, and the maximum inter-story drift of the structure was 1/203, indicating that the steel frame has good capacity to resist the lateral deformation.

• The response of acceleration and displacement of the steel frame increased with the increase of peak acceleration of seismic waves. The time at which the maximum response appeared was different from that of the peak acceleration of input wave.

• Under Wenchuan wave with the peak acceleration of 620 gal, the steel frame began to enter the yield stage without the obvious buckling and instability, which shows that the steel frame with archaized-style has good seismic performance and security reserve.

• The weak zones of the steel frame are Dou-Gong and beam ends at both sides of Dou-Gong of column Z-2. Dou-Gong, beam ends and column bottom ends yielded in turn, meeting the seismic resistance requirements of "strong-column and weak-beam".

• Dou-Gong plays an important role on seismic performance of the steel frame with archaized-style, and it is the first line of seismic fortification for the steel frame.

Acknowledgements

This work presented in this paper was supported by the National Natural Science Foundation of China (Grant no. 51208411), Key Science and Technology Innovation Team of Shaanxi Province (2019TD-029) and Technology Research Task of China State Construction Engineering Corporation (Grant no. CSCEC-2012-Z-16).

Reference

Blum, H.B. and Rasmussen, K.J.R. (2019), "Experimental and numerical study of connection effects in long-span cold-formed steel double channel portal frames", *J. Constr. Steel Res.*, **155**, 480-491. https://doi.org/10.1016/j.jcsr.2018.11.013.

Cheng, M. and Wen, G. (2017), "Seismic behavior comparison of lateral force resisting system of steel structure", *World Inform. Earthq. Eng.*, **33**(1), 244-251.

Dan, D. (2008), "Behavior and performance of cold-formed steel-frame houses under seismic action", *J. Constr. Steel Res.*, **64**(7), 896-913. https://doi.org/10.1016/j.jcsr.2008.01.029.

Gattesco, N. and Boem, I. (2015), "Seismic performances and behavior factor of post-and-beam timber buildings braced with nailed shear walls", *Eng. Struct.*, **100**(1), 674-685. https://doi.org/10.1016/j.engstruct.2015.06.057.

Ghasem, D.A. (2018), "A performance based strategy for design of steel moment frames under blast loading", *Earthq. Struct.*, **15**(2), 155-164. https://doi.org/10.12989/eas.2018.15.2.155.

Jiang, S.F., Wu, M.H., Tang, W.J. and Liu, X.M. (2016), "Multi-scale modeling method and seismic behavior analysis for ancient timber sutrctures", *J. Build. Struct.*, **37**(10), 44-53.

Li, C.H., Tsai, K.C., Su, L. and Lin, P.C. (2018), "Experimental investigations on seismic behavior and design of bottom vertical boundary elements in multi-story steel plate shear walls", *Earthq. Eng. Struct. Dyn.*, **47**(14), 2777-2801. https://doi.org/10.1002/eqe.3106.

Lian, M., Su, M.Z. and Guo, Y. (2017), "Experimental performance of Y-shaped eccentrically braced frames fabricated with high strength steel", *Steel Compos. Struct.*, **24**(4), 441-453. https://doi.org/10.12989/scs.2017.24.4.441.

Negin, S., Karin, A., Mehdi, P. and Hassan, G. (2017), "An investigation of seismic parameters of low yield strength steel plate shear walls", *Earthq. Struct.*, **12**(6), 713-723. https://doi.org/10.12989/eas.2017.12.5.713.

Parisi, M.A. and Piazza, M. (2015), "Seismic strengthening and seismic improvement of timber structures", *Constr. Build. Mater.*, **97**(30), 55-65. https://doi.org/10.1016/j.conbuildmat.2015.05.093.

Qi, L.J., Xue, J.Y. and Leon, R.T. (2017), "Experimental and analytical investigation of transition steel connections in traditional-style buildings", *Eng. Struct.*, **150**, 438-450. https://doi.org/10.1016/j.engstruct.2017.07.062.

Sakr, M.A., Eladly, M.M., Khalifa, T. and El-Khoriby, S. (2019), "Cyclic behavior of infilled steel frames with different beam-to-column connection types", *Steel Compos. Struct.*, **30**(5), 443-4566. https://doi.org/10.12989/scs.2019.30.5.443.

Wang, Y.B., Li, G.Q. and Cui, W. (2014), "Seismic behavior of high strength steel welded beam-column members", *J. Constr. Steel Res.*, **102**, 245-255. https://doi.org/10.1016/j.jcsr.2014.07.015.

Wu, X.Y. (2010), "Mechanical properties of Dingding gate steel structure component", Master Dissertation, Chang'an University, Xi'an, China. (in Chinese)

Wang, L. (2012), "Comparative study on structural behavior between ancient structure and antique building of a Qing-style Hall", Master Dissertation, Xi'an University of Architecture and Technology, Xi'an, China. (in Chinese)

Xue, J.Y., Ma, L.L., Wu, Z.J. and Gao, W.X. (2018), "Influence analysis of bracket set on seismic performance of steel eave columns in Chinese traditional style buildings", *Struct. Des. Tall Spec. Build.*, **27**(8), e1462. https://doi.org/10.1002/tal.1462.

Xue, J.Y., Wu, Z.J., Sui, Y. and Liu, Z.Q. (2015), "Experimental study on seismic performance of steel double-beams column exterior joints in antique style building", *J. Build. Struct.*, **36**(3), 80-89.

Zhang, X.C., Xue, J.Y., Zhao, H.T. and Sui, Y. (2011), "Experimental study on Chinese ancient timber-frame building by shaking table test", *Struct. Eng. Mech.*, **40**(4), 453-469. https://doi.org/10.12989/sem.2011.40.4.453.

CC